

Original Article

Cite this article: Azizi A, El Albani A, El Bakhouche A, Vinn O, Bankole OM, Fontaine C, Hafid A, Kouraiss K, and El Hariri K (2023) Early biomineralization and exceptional preservation of the first thrombolite reefs with archaeocyaths in the lower Cambrian of the western Anti-Atlas, Morocco. *Geological Magazine* **160**: 428–443. <https://doi.org/10.1017/S0016756822001017>

Received: 22 February 2022
Revised: 2 September 2022
Accepted: 3 September 2022
First published online: 18 October 2022



Keywords:

bacterial fossils; nanoglobules; pyrite framboids; *Renalcis*

Author for correspondence:

A. Azizi,
Email: a.azizi@uca.ma

Early biomineralization and exceptional preservation of the first thrombolite reefs with archaeocyaths in the lower Cambrian of the western Anti-Atlas, Morocco

Abdelfattah Azizi¹ , Abderrazak El Albani², Asmaa El Bakhouche¹, Olev Vinn³ , Olabode M. Bankole², Claude Fontaine², Ahmid Hafid¹, Khaoula Kouraiss¹ and Khadija El Hariri¹

¹Département de Géologie, Faculté des Sciences et Techniques, Université Cadi-Ayyad, BP 549, 40000 Marrakesh, Morocco; ²Laboratoire IC2MP 7285 CNRS-INSU, Université de Poitiers, 86022 Poitiers, France and ³Department of Geology, University of Tartu, Ravila 14A, 50411 Tartu, Estonia

Abstract

Thrombolite reefs with archaeocyaths are common in the subtidal limestones of the lower Cambrian in the western Anti-Atlas of Morocco. The Igoudine Formation of the Tata Group recorded the first replacement of the microbial consortium (stromatolite-dominated) by thrombolite reefs with archaeocyaths and shelly metazoans. In order to better understand the role of the microbial community in the formation of thrombolite reefs with archaeocyaths across this critical transition, the macro-, micro- and ultra-fabric of thrombolites have been studied in detail. Three major components are identified within the first thrombolytic reef: archaeocyaths, calcimicrobes and micritic matrix. The studied thrombolites are typically dominated by the calcimicrobe *Renalcis* with subordinate *Epiphyton* and *Girvanella*. Scanning electron microscopy of the dark micrite of the *Renalcis* chambers showed amorphous translucent sheet-like structures interpreted as extracellular polymeric substances, closely associated with organominerals including nanoglobules and polyhedrons. Exceptionally well-preserved *Renalcis* chambers contain bacterial fossils similar to those described in modern microbialites, including microspherical coccoid fossils and filamentous bacteria that are either spaced or in close associations forming colonies. These organomineralization-related features suggest a bacterial origin for the *Renalcis* calcimicrobe. The matrices between the *Renalcis* chambers consist predominantly of clotted peloidal micrite. Mineralization of *Renalcis* microframes may involve two major biomineralization processes: (1) replacement of organic matter by organominerals resulting from anaerobic degradation of extracellular polymeric substances and bacterial sheaths and (2) encrustation of bacterial sheaths and extracellular polymeric substances due to increasing alkalinity of the microenvironment. These mechanisms played a crucial role in the early diagenetic cementation and preservation of the studied reefs.

1. Introduction

Thrombolites are benthic microbial carbonates recognized by their patchy mottled/clotted structures with no internal lamination (Aiken, 1967; Tang *et al.* 2012) and are composed of calcimicrobes, micrite and peloids (Riding, 2008). Kershaw *et al.* (2007) applied the term digitate dendrolite to Permian–Triassic boundary microbialites in Sichuan, China. However, Riding (2011) presented a plausible argument that a dendrolitic form seen in vertical section may also be classified as a thrombolite because in transverse section the branched structure appears as clots on a cut surface (Riding, 2011; Kershaw *et al.* 2021). Thrombolites are found globally in various modern depositional environments such as open subtidal settings (Planavsky & Ginsburg, 2009; Myshrall *et al.* 2010; Mobberley *et al.* 2012), freshwater (Laval *et al.* 2000; Gischler *et al.* 2008), alkaline (Arp *et al.* 2003) and hypersaline (Puckett *et al.* 2011) lakes, and hot springs (Campbell *et al.* 2008). Early works suggested that the clotted fabrics of thrombolites may have resulted from the destruction of stromatolitic laminae by metazoans or diagenesis (Hofmann, 1973; Walter & Heys, 1985). Research on modern thrombolites in the Bahamas (Highborne Cay; Myshrall *et al.* 2010), Australia (Shark Bay; Jahnert & Collins, 2012) and Kuwait (Arabian Gulf; AlShuaibi *et al.* 2015) have improved our knowledge of these kinds of calcareous microbialites and also confirmed their primary biogenic origin. Similar to other microbialites, thrombolites are formed from complex interactions between microbial communities and the surrounding waters, whereas microbially induced calcification and/or trapping and binding of sediments are the most important processes involved in their growth

and expansion (Burne & Moore, 1987; Riding, 2000; Planavsky & Ginsburg, 2009; Jahnert & Collins, 2012).

The lower Cambrian deposits in Morocco are widely exposed in the Anti-Atlas belt and High Atlas Mountains (Álvaro *et al.* 2014). During this period, the marine platform of the Anti-Atlas was part of the northern margin of the Gondwana supercontinent. Microbial reefs (dominated by stromatolites) remained unaffected until the early Cambrian Stage 3 (Atdabanian). During the formation of the Tiout Member (upper unit of the Igoudine Formation) an important palaeoecological event took place, characterized by the replacement of the microbial consortium (stromatolite-dominated) by thrombolites and shelly metazoans (Hupé, 1960; Schmitt & Monninger, 1977; Schmitt, 1979; Destombes *et al.* 1985; Debrenne & Debrenne, 1995; Álvaro & Clausen, 2006; Álvaro & Debrenne, 2010; Clausen *et al.* 2014). Several authors have mentioned the first episode of thrombolite reefs with archaeocyaths in the lower Cambrian (Series 2) Tiout Member in the western Anti-Atlas (Benssaou & Hamoumi, 2004; Álvaro & Debrenne, 2010; Álvaro *et al.* 2014); however, the detailed study and interpretation of this event is still lacking. The current work is focused on the details of the structures, mineralogy and geochemistry, providing a genesis model for the first thrombolite reef complex containing archaeocyaths in the lower Cambrian of Morocco.

2. Geological setting and stratigraphy

The Anti-Atlas Mountains are a c. 1300 km long NE–SW-trending belt in the central part of Morocco (Fig. 1a, b). The southern slope of the Anti-Atlas contains well-exposed Palaeozoic sedimentary successions resting on the Precambrian Pan-African orogen (Destombes *et al.* 1985; Geyer & Landing, 1995). It comprises a ~1800 m thick mixed siliciclastic-carbonate deposit on the north Gondwana margin (western Anti-Atlas, Morocco) directly deposited on the ~2000 m thick volcanic and volcanoclastic rocks of the Ediacaran Ouarzazate Supergroup (577–560 Ma) (Thomas *et al.* 2004; Gasquet *et al.* 2008; Walsh *et al.* 2012; Fig. 1b). This Ediacaran–Cambrian succession accumulated on the thermally subsiding continental shelf (Maloof *et al.* 2005) in the upper part of the eastern Anti-Atlas platform. The Tata Group is well exposed in the Taroudant province, and has previously been described in the Tiout, Amouslek and Tazemmourt areas (Álvaro *et al.* 2006), and within the Issafen and Fouanou synclines. The ~1000 m thick Tata Group consists of four formations: Igoudine, Amouslek, Issafen and Asrir (Fig. 1c). The basal Igoudine and Amouslek deposits represent carbonate-dominated environments such as peritidal flats and ooid shoals. The upper part of the Igoudine Formation has been described only in the Tiout area as the Tiout Member (Álvaro *et al.* 2006), containing the boundary interval where the microbial consortium (stromatolite-dominated) sediments were first replaced by thrombolite reefs with archaeocyaths and shelly metazoans (Álvaro *et al.* 2014). The thickness of the overlying Amouslek Formation ranges between 20 and 220 m and consists of variegated shales with interbedded limestones.

The Tommotian–Atdabanian boundary interval is widely exposed in the western Anti-Atlas (Fouanou syncline). One characteristic section comprising the Igoudine and Amouslek formations has been logged by us (Fig. 1d). The stratigraphic succession in this area comprises similar sedimentary facies to those described within the type sections of the Tiout and Amouslek areas (Álvaro *et al.* 2006; Álvaro & Debrenne, 2010).

The lowermost unit of Igoudine Formation (~40 m thick) consists of massive black oolitic limestones, with rare dome-shaped stromatolites, symmetric ripples and cross-stratifications. In the middle unit (~35 m thick) dominated by stratified dolostones, displaying crinkled dome-shaped and stratiform stromatolites, wave ripples and rare cross-stratifications, horizons shows slumped and faulted stromatolites. Based on the sedimentary facies, both previous units were deposited in upper subtidal to intertidal environments. The upper unit of the Igoudine Formation formed by massive bedded oolitic limestone ('black oolitic limestone facies' of Monninger, 1979 and Schmitt, 1979) is characterized by the emergence of small-sized archaeocyaths, Atdabanian in age, including *Dictyocyathus*, *Erismacoscinus* and *Agastrocyathus*. Some beds exhibit cross-stratifications and rare wave ripples and erosion surfaces. The latter unit is overlain by the Tiout Member dominated by dendritic thrombolites with archaeocyaths, which is the first microbial archaeocyathan reef barrier of the Anti-Atlas. Thrombolite–archaeocyathan reefs are characterized by successive reef-growth phases delimited by surfaces of reef-growth interruption, which suggest that this reef barrier may have formed under low-energy conditions with occasional high-energy events, generating erosion surfaces. The latter conditions can occur between the middle to lower subtidal zone (Jahnert & Collins, 2012). The Amouslek Formation consists of variegated shales and siltstones, strongly bioturbated, recording a significant sea-level change from shallow water restricted conditions to deeper open sea conditions (Álvaro & Debrenne, 2010). The lower part of this unit displays numerous archaeocyathid-bioherms and patch reefs. The upper part consists mainly of shales and fine-grained sandstones with interbedded oolitic limestones, cross-stratifications and wave ripples, recording rhythmic transgressive–regressive depositional sequences.

3. Materials and study methods

Thrombolites were macroscopically examined in the field and in polished slabs in the laboratory. About 70 thin-sections were made for microfacies analyses using an Olympus BH2 polarizing binocular microscope. Platinum-coated and uncoated freshly broken sample fragments were observed for micro/nanostructures using an FEI Teneo Volume Scope scanning electron microscope (SEM), operated at a 5 to 20 kV accelerating voltage and a varying working distance of between 9 and 11 mm, at UFR SFA Pole Biology University of Poitiers, France. Semi-quantitative element analyses of sub-micron-sized spots were determined using an EDAX energy-dispersive X-ray spectrometer (EDS) connected to the SEM at 20 kV and a working distance of 9 mm. The bulk mineral compositions of some thrombolite fragments from the bottom and upper part of the lower reef complex of the Igoudine Formation were determined using a Bruker D8 ADVANCE X-ray diffractometer (CuK α radiation) with operating conditions of 40 kV and 40 mA and a 0.025/s step size.

4. Results

4.a. Thrombolytic reefs with archaeocyaths

4.a.1. Morphology and macrofabric

Thrombolite–archaeocyathan reefs of the Igoudine Formation are characterized by successive reef-growth phases delimited by surfaces of reef-growth interruption (Fig. 2a). The Atdabanian thrombolites of the Igoudine Formation exhibit dark micritic mesoclots

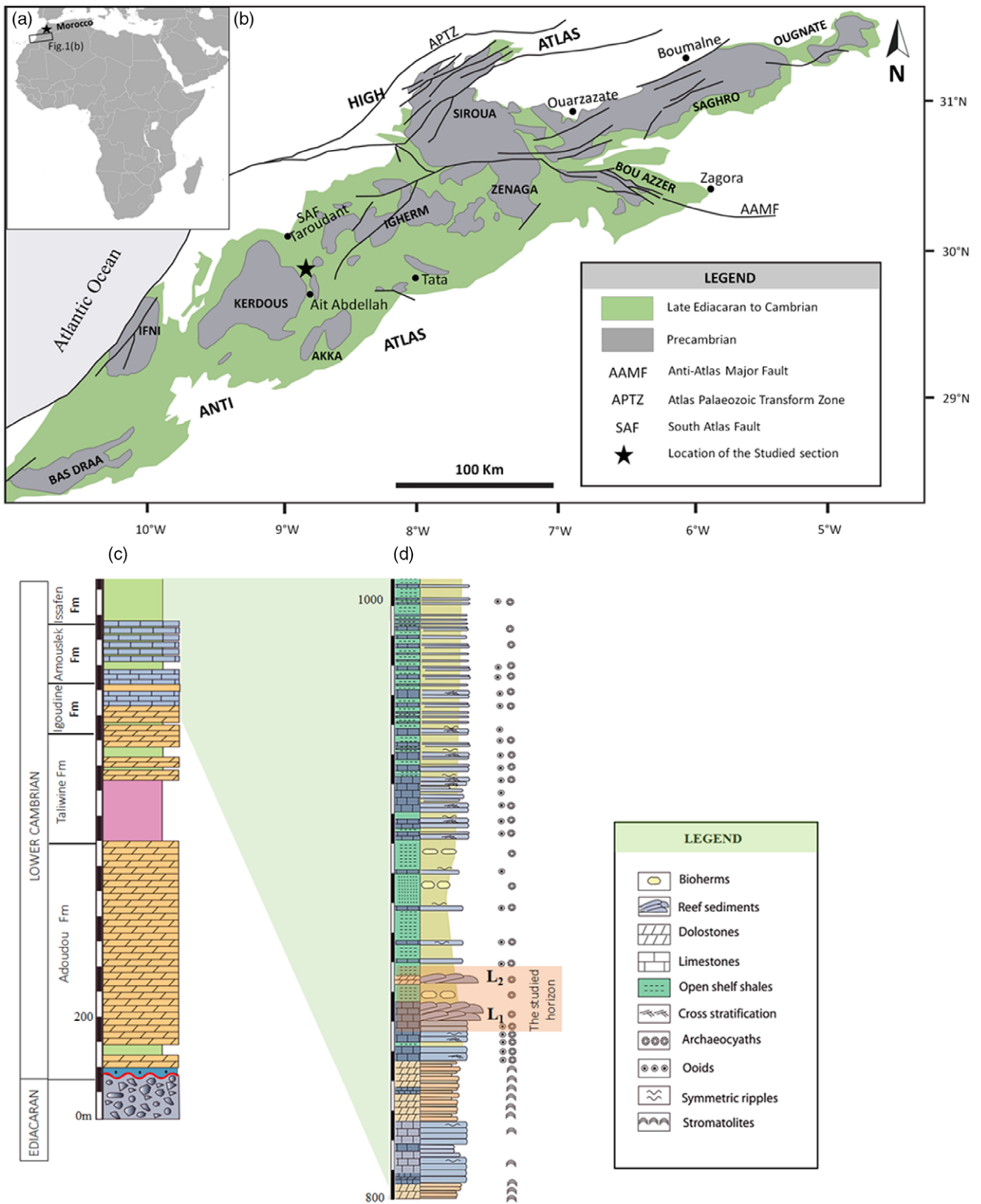


Fig. 1. (Colour online) (a) Location map of the Anti-Atlas of Morocco. (b) Simplified geological sketch showing the distribution of the Precambrian–Cambrian outcrops in the Anti-Atlas Mountains (drawn after Saadi et al. 1983). (c) Stratigraphic section through the lower Cambrian of the Fouanou syncline. (d) Detailed lithostratigraphic section of the studied horizon in the Fouanou syncline (the diameters of archaeocyath cups were measured within the levels L1 and L2).

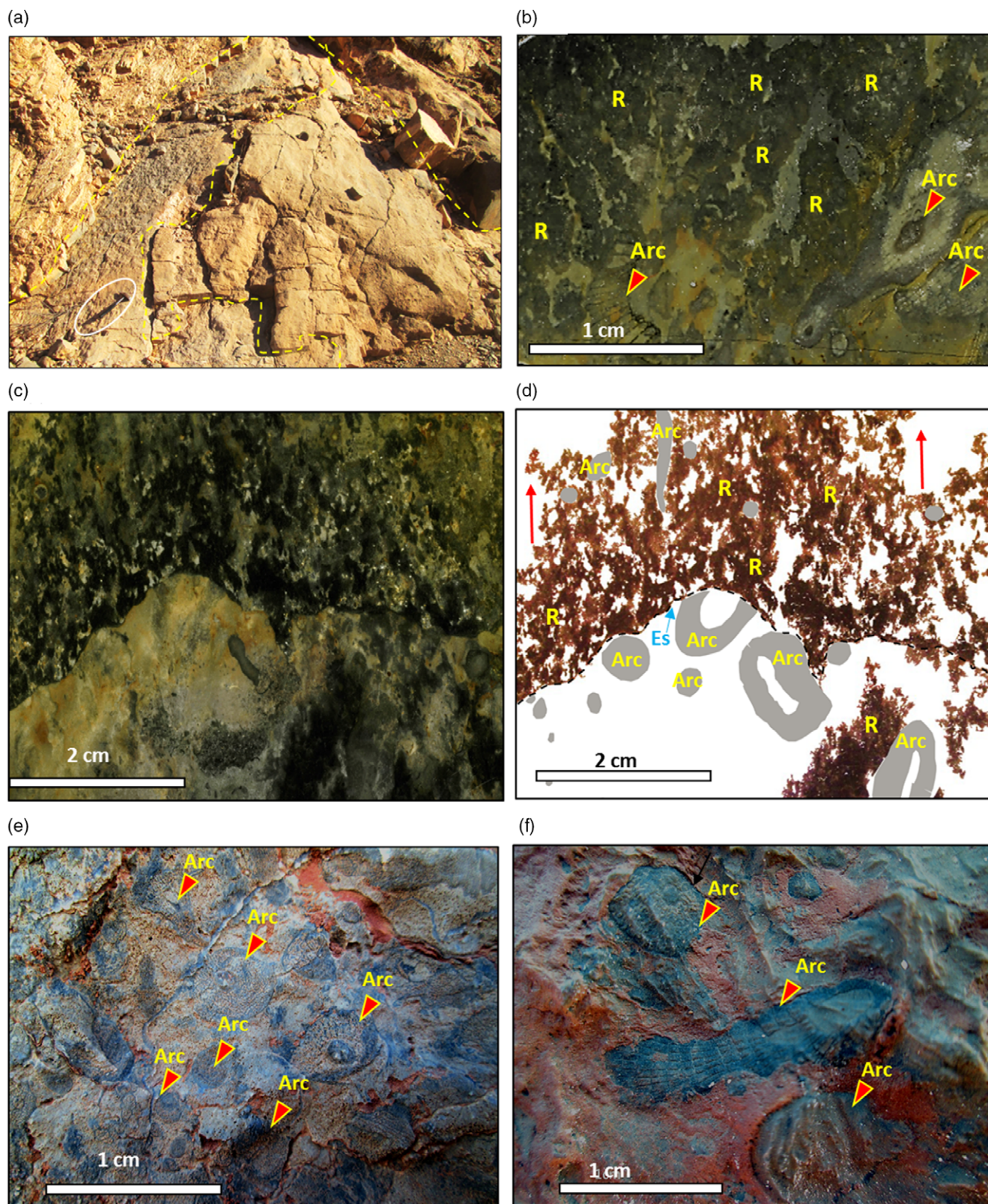


Fig. 2. (Colour online) Macroscopic features of the thrombolite reef with archaeocyaths. (a) Outcrop photograph of thrombolite–archaeocyathan reefs characterized by successive reef-growth phases delimited by surfaces of reef-growth interruption (length of hammer scale is 29.5 cm). (b) Sample slab showing dark grey dendritic mesoclots and light grey matrix with scarce archaeocyaths (Arc). (c, d) Photographs and sketches of longitudinal section showing dendritic clotted fabric growing upwards (red arrows) (Arc – archaeocyath; Es – erosion surface). (e, f) Photographs of transverse sections showing small-sized regular and irregular archaeocyaths (Arc).

in varying sizes and shapes and have maximum diameters ranging between 5 and 20 mm (Fig. 2a, b). The mesoclots are interlaced to form upward-growing dendritic structures (Fig. 2b, c, d). Scattered small-size archaeocyaths are apparent within the studied materials (Fig. 2b, c, d, e, f), but they never exceed 20 % of the total rock volume. Three genera have been identified in the studied horizon including *Dictyocyathus*, *Erismacoscinus* and *Agastrocyathus*. They are usually less than 20 mm in height and preserved in their growth position. The maximum diameters of 150 cups of archaeocyaths measured within two spaced reef cores (Fig. 2b) vary from 1 to 31 mm with a mean of 4.9 mm in the lower level (L₁) and from 2 to 47 mm with a mean of 5.6 mm in the upper level (L₂) (Fig. 3). Dendritic thrombolites in the lower Cambrian Series 2 of the Founou syncline show well-preserved calcimicrobes such as *Renalcis*, *Epiphyton* and *Girvanella*.

4.a.2. Microscale characteristics

Dendritic thrombolites display well-defined clots containing numerous calcimicrobes, including *Renalcis*, *Epiphyton* bundles and subordinate *Girvanella* tubes visible in thin-sections (Fig. 4a). The *Renalcis* group is the most abundant dendritic microbial fossil recorded within the studied reefs, consisting of a growing-upward shrub-like array of connected chambers made up of aphanitic micrite (Fig. 4a, b). Micrites, microspar and rare scattered clotted peloids (50 to 100 µm thick) filled the voids separating the *Renalcis* microframes. The diameters of the chambers range from 0.2 to 1.5 mm, and they commonly occupy the void spaces between the archaeocyath skeletons (Fig. 2c). Calcified microbial thrombolites show a tabular morphology. The *Epiphyton* calcimicrobe occurs in archaeocyath dominated reefs, encrusting the archaeocyath skeleton (Fig. 4c, d). They are observed as radiating branches consisting of aphanitic micrites and are usually grouped in relatively large colonies (up to 5 mm in diameter) to form a chambered structure (Fig. 4c, d), similar to *Renalcis*. However, it is difficult to distinguish between both structures in some cases, especially when the filaments are densely connected. Spaced *Girvanella* tubes are rare and usually separated from the *Renalcis* and *Epiphyton* microframes. The light grey matrix surrounding the *Renalcis* and *Epiphyton* frameworks consists of micrite and microspar with randomly scattered dark grey micritic peloid-like aggregates with diffuse edges (Fig. 4e, f). Irregular cavities and geopetal structures are common and are filled by greyish microspar or fibrous calcite.

4.a.3. The nature of the matrix

The matrices between the *Renalcis* and *Epiphyton* chambers consist predominantly of clotted micrite and microspar, occurring as scattered poorly sorted peloid 'grainstone-packstone' (Fig. 4e, f). Allochthonous fine silt particles, including recognizable quartz and feldspar, are locally incorporated into the thrombolite but are generally scarce and only visible in samples taken beneath the Amouslek Formation shales. The size of the peloids that dominate the matrix microfabric mostly range between 30 and 80 µm. The high-density and coarse-grained peloids are common within the empty spaces between the *Renalcis* chambers (Fig. 4a, e, f). Some peloids show well-defined boundaries with simple outlines, scattered within the microspar matrix. However, other peloids exhibit irregular forms and occur as clotted aggregates with no well-defined margins. In contrast, the fine-grained peloids are spaced relatively far from the *Renalcis* microframes (Fig. 4b, e). The *Renalcis* and *Epiphyton* chambers also host the fine-grained peloids but in a lower density. A little pyrite also occurs within

the matrix under reflected light and is surrounded by a cloud of iron oxides (Fig. 4f).

4.b. Ultra-fabrics of thrombolites

SEM observations of the *Renalcis* and *Epiphyton* chambers revealed amorphous translucent sheet-like structures interpreted as extracellular polymeric substances (EPSs) (Arp et al. 2001; Decho et al. 2005; Barrett et al. 2009; Mishra et al. 2009; Jones, 2011; Zatoń et al. 2012; Zhang et al. 2015; Mackey et al. 2017). Interpreted bacterial remains, pyrite framboids and a closely associated organomineral complex (biologically induced and biologically influenced mineralization), including nanoglobules, polyhedrons and micropeloids, are scattered within the interpreted mineralized EPS matrix.

4.b.1. Extracellular polymeric substances (EPSs)

The EPSs show an amorphous flat and translucent mucus-like matrix (Fig. 5a, b, c) and form a meshwork of subpolygonal pits and walls (1–3 µm thick; Fig. 5a). EDS analyses show that the EPS matrix is composed of C, O, Ca, Si, Mg, Al, K, Cl and rare detectable Fe and S (Fig. 5b, d, e, f). The EPS surface in some areas shows nano-sized cracks (Fig. 6a). Rod-like forms and uniform spherical bodies are similar to those that have been reported in microbialites in many areas and interpreted as bacterial fossils (Perri & Tucker, 2007; Spadafora et al. 2010; Perri et al. 2012; Shen et al. 2017). Bacterial fossils are commonly attached or entombed within the EPS films in the well-preserved samples of *Renalcis* chambers (Figs 5c, 6b, c, d, e, f). These bacterial cell remains are mainly composed of filamentous and micro-spherical forms and are separated into filamentous tube-like fossils and filamentous rod-like to slightly ellipsoidal-shaped forms based on their different shapes and dimensions. The filamentous tube-like fossils have slightly curved tubes and are either isolated or grouped forming colonies (Figs 5c, 6b, c, d). The filamentous rod-like to slightly ellipsoidal-shaped cells (250–300 nm long and 50 nm wide) are usually found in associations to form colony-like clusters, up to 5 µm in diameter (Fig. 6c, d). Nanoscale SEM observations show the presence of fine granular textures on the surfaces of the possible bacteria fossils (Fig. 6c, d). Micro-spherical forms interpreted as coccoids, with uniform diameters of 600 nm, are grouped in colonies probably associated with irregular organic fragments (Fig. 6c, d).

4.b.2. Organomineral complex

Higher magnification SEM observations of *Epiphyton* and *Renalcis* chambers and the clotted peloids show abundant nanoglobules that are 40–80 nm in size (Fig. 7a, b, c, d, e, f) and often fused into clusters to form anhedral polyhedrons of various sizes, depending on the number of the associated aggregates (Fig. 7a, b, c). The polyhedrons coalesce into irregular micrometre-scale micropeloids. The nanoglobules are closely related to EPS relics or clustered on their surfaces (Fig. 7e, f).

4.b.3. Framboidal pyrite

Pyrite framboids are common in the dark micrite forming the *Renalcis* and *Epiphyton* chambers. They are embedded in platy or amorphous EPSs (Fig. 8a, b, c). The diameter of the framboids varies between 4 µm and 40 µm, and they form euhedral (octahedral) microcrystals of 0.5–2 µm in size. The framboidal pyrite entombed in EPS relics contains Fe, S and Ca (Fig. 8d).

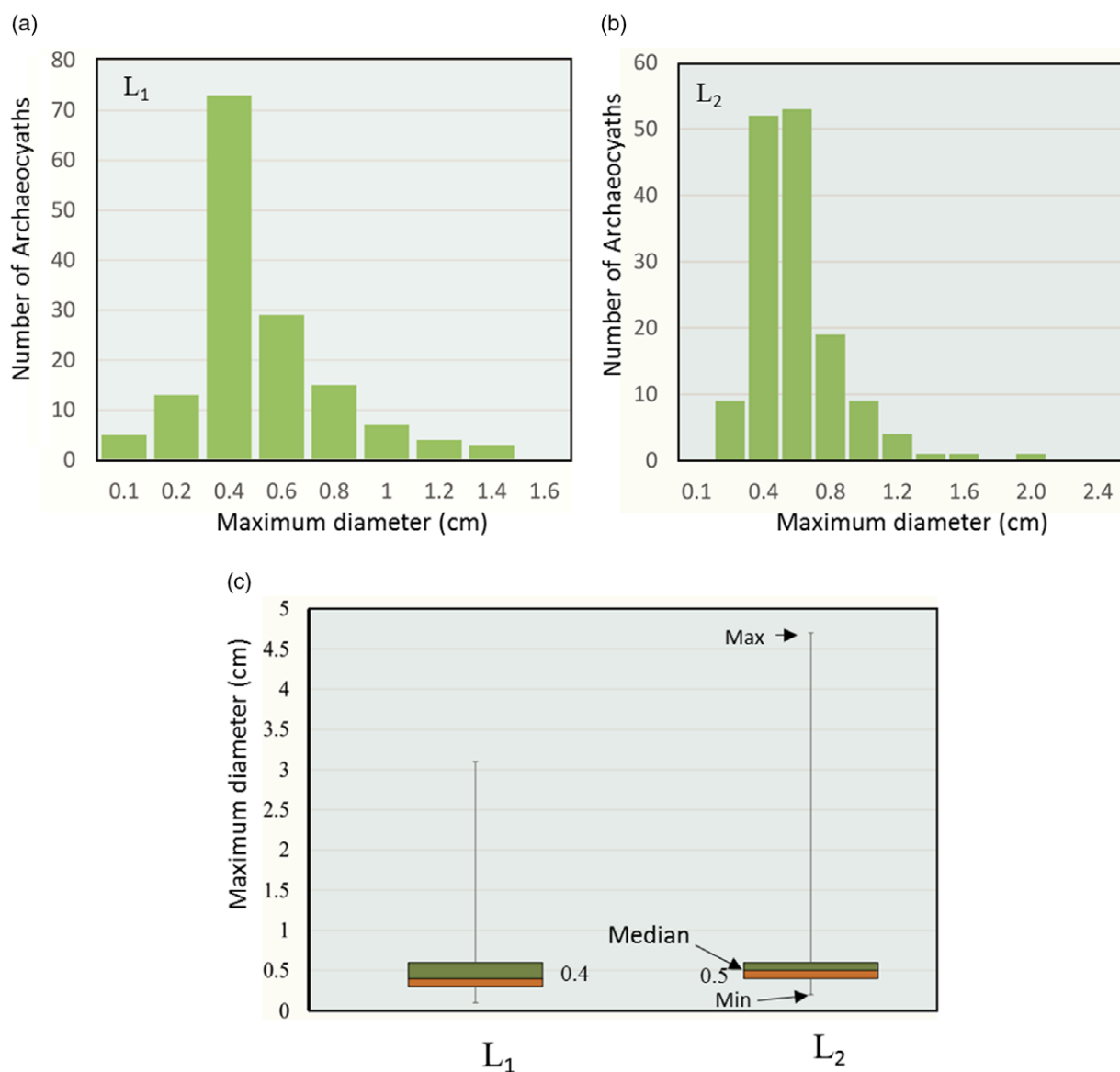


Fig. 3. (Colour online) Distribution patterns of the maximum diameter of 150 cups of archaeocyaths measured within two spaced levels (a) L₁ and (b) L₂ (shown in Fig. 1d). (c) Box-plots of cup diameters in both L₁ and L₂.

4.c. Mineralogical composition of thrombolites

Mineralogical compositions of the thrombolite sediments show differences between the bottom and the top of the lower reef complex (Fig. 9a, b). Samples from the basal parts of the section contained mainly carbonate and a small amount of quartz and pyrite (Fig. 9a). However, the upper part of the complex, beneath the Amouslek calcareous shales, is dominated by carbonate and siliclastic minerals represented by feldspar, mica, silica and a small amount of pyrite (Fig. 9b).

5. Discussion

5.a. Components of thrombolite reefs

Early Cambrian microbial reefs containing archaeocyaths have been reported globally (Debrenne *et al.* 1989; Rees *et al.* 1989; James & Gravestock, 1990; Gandin & Luchinina, 1993; Gandin & Debrenne, 2010). In the Anti-Atlas, stromatolite-dominated

microbial reefs remained unaffected until early Cambrian (Atdabanian) time, when thrombolite reefs with archaeocyaths became widespread (Álvaro & Debrenne, 2010). These changes could be related to sea-level fluctuation, from shallow water restricted to deeper open sea conditions (Álvaro & Debrenne, 2010).

The scattered small size of the archaeocyaths, their preservation in life position, microbial fabric attachments to *Renalcis* microframes, encrustation by *Epiphyton* chambers and a *Girvanella* crust, as well as their lower abundance (~20%) in thrombolite reefs ecosystems, suggest that they were reef dwellers rather than local framework builders. They usually required the presence of microbial elements to form frameworks (Debrenne, 2007). Archaeocyath-*Renalcis*-*Epiphyton* reefs occur in low-energy subtidal conditions, mostly from lower subtidal to the outer ramps (Debrenne *et al.* 2002; Gandin *et al.* 2007), but they are also present on high-energy platform margins (Kruse *et al.* 1995; Riding & Zhuravlev, 1995). The

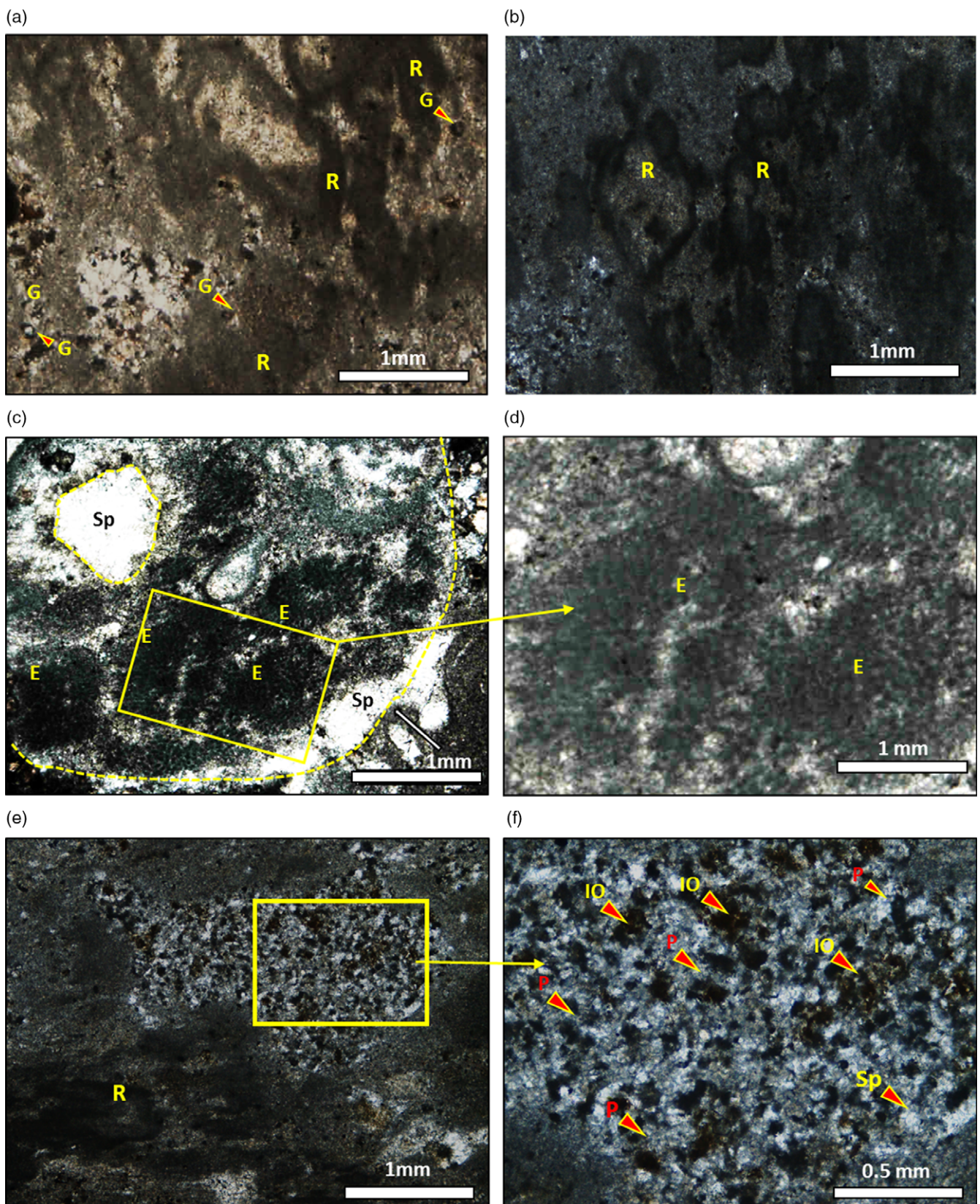


Fig. 4. (Colour online) Microscopic features of thrombolites observed under plane-polarized light. (a, b) Micrographs showing the various forms of *Renalcis* chambers (R) and *Girvanella* tubes. (c) Photomicrograph showing *Epiphyton* chambers (E) attached to archaeocyaths and surrounded by sparitic matrix (Sp). (d) A close-up view of the boxed area in (c) showing *Epiphyton* chambers with radiating filaments. (e) Photomicrograph of peloidal fabrics in the cryptic space between *Renalcis* chambers. (f) A close-up view of the boxed area in (e) showing the peloid (P) microspar fabric with a rare cloud of iron oxides (IO) derived from pyrite oxidation.

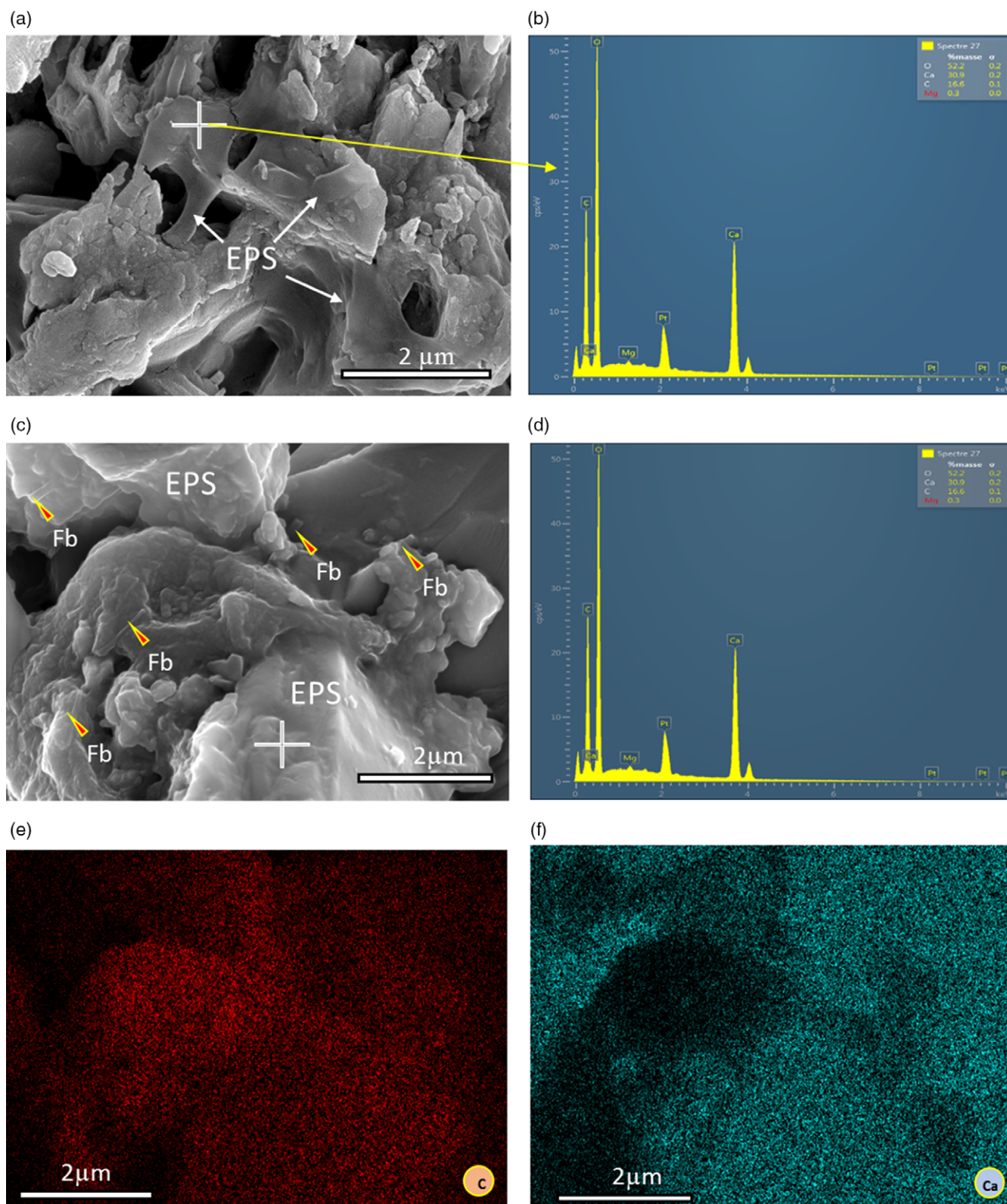


Fig. 5. (Colour online) Scanning electron microscopy photomicrographs and EDS of microbial structures in the micritic *Renalcis* chamber. (a) Close-up view of honeycomb-like structure consisting of translucent polygonal pits and walls interpreted as mineralized extracellular polymeric substance (EPS) matrix. (b) EDS spectrum and elemental quantitative data of the spot in (a). (c) EPS relics containing filamentous bacteria (Fb). (d) EDS spectrum and elemental quantitative data of the surface shown in (c) (Pt element resulted from platinum coating). (e, f) Elemental mappings of carbon (C) and calcium (Ca) of the surface in (c).

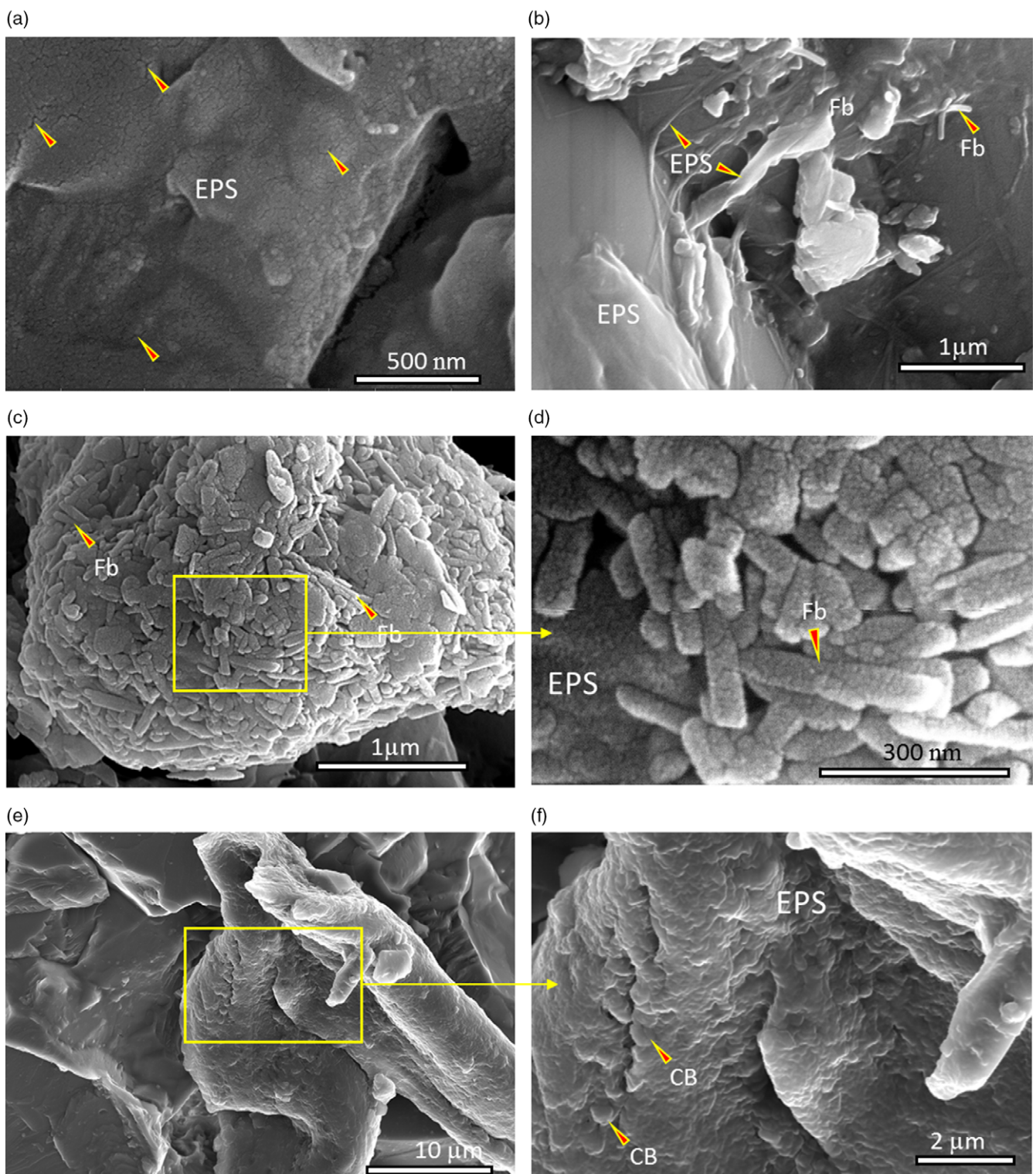


Fig. 6. (Colour online) Scanning electron microscopy photomicrographs of EPSs and bacterial fossils. (a) EPSs showing nano-sized cracks that possibly result from dehydration of EPS films during early diagenesis. (b) EPS relics coating micrite crystals with filamentous bacterial fossils. (c) Filamentous bacteria (Fb) grouped in a colony. (d) Magnified view of the boxed area in (c) showing the fine granular texture of the surface of bacteria with nano-sized cracks. (e) Grainy surface on possible organic residue. (f) Magnified view of the boxed area in (e) showing the micro-spherical form of possible coccoidal bacteria (CB) covering the surface of organic remains and associated mineralized EPSs.

incorporation of fine-grained sediments into the thrombolite reefs suggests that they formed under low-energy conditions. The presence of erosion surfaces (Fig. 2a, c, d) indicates that reef growth was likely interrupted by episodic storm events.

The remarkable change in diameter of archaeocyaths between both horizons L_1 and L_2 (Fig. 1d) could be related to variations in the chemical and/or hydrodynamic conditions of the environment.

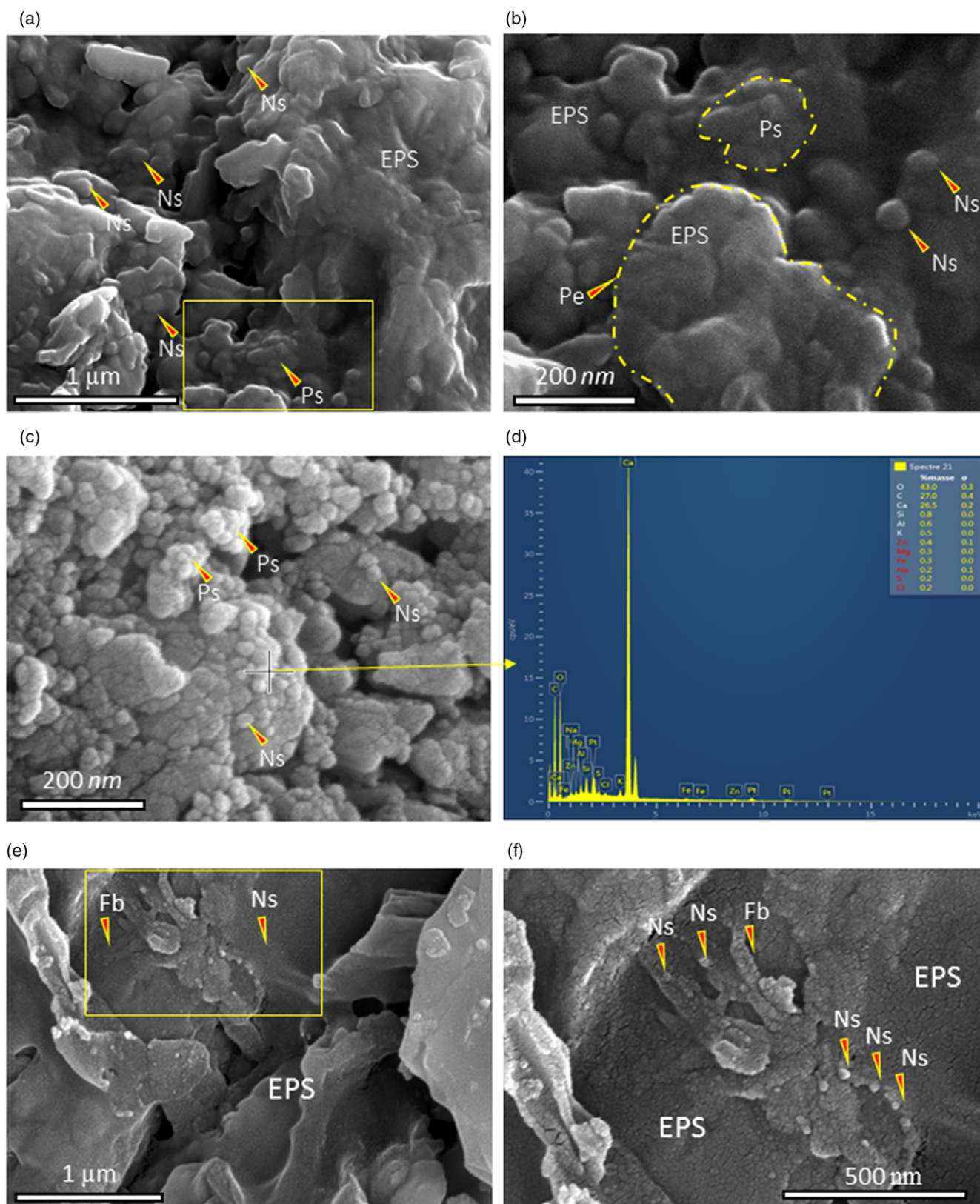


Fig. 7. (Colour online) Scanning electron microscopy photomicrographs showing organominerals and detrital micrite in thrombolites. (a) Scattered nanoglobules (Ns) coalesced to form polyhedrons (Po) within EPS films. (b) Magnified view of the boxed area in (a) showing nanoglobules (Ns) and polyhedrons (Po) fused into micropeloids (Pe), closely associated with EPS relics. (c) Nanoglobules (Ns) coalesced to form polyhedrons (Po) and irregular micritic particles. (d) EDS spectrum and elemental quantitative data for nanoglobules (analysed spot (+) in (c)) (Pt element resulted from platinum coating). (e) Nanoglobules closely associated with EPSs and the probable filamentous bacteria (Fb). Nanoglobules (Ns) are visible on EPS flats. (f) Magnified view of the boxed area in (e) showing nanoglobules and nano-cracks resulting from dehydration of EPSs during early diagenesis.

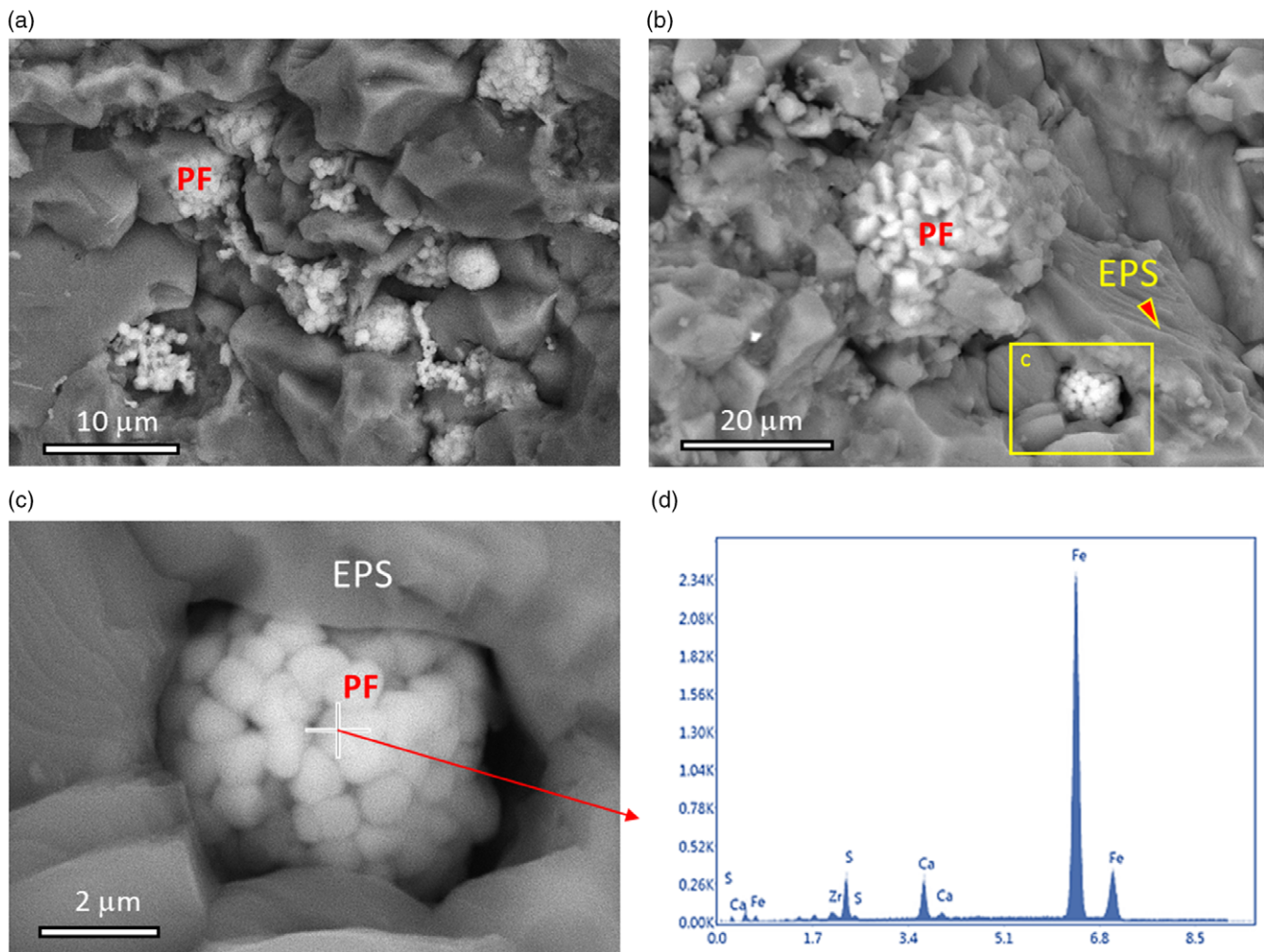


Fig. 8. (Colour online) Scanning electron microscopy photomicrographs of pyrite framboids. (a, b) Abundant pyrite framboids (PF) consisting of equidimensional pyrite microcrystals associated with mucus-like EPS relics. (c) Close-up view of the boxed area in (b) showing pyrite framboid. (d) EDS spectrum of pyrite crystal in (c) (+ indicates the position of analysed spot). Fe, S and Ca elements are common in the pyrite crystals.

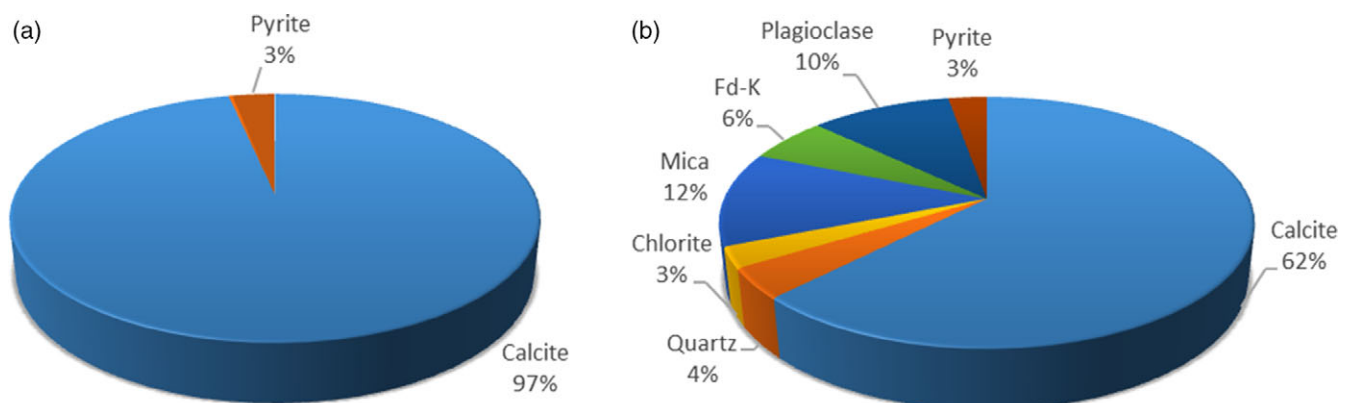


Fig. 9. (Colour online) Bulk rock mineralogical composition of selected samples from (a) the bottom and (b) the top of the lower reef complex of the Igoudine Formation (see Fig. 1d).

The Igoudine thrombolite reefs are composed of calcimicrobes: *Renalcis* with subordinate *Epiphyton* and *Girvanella* (Fig. 4a, b, c, d). The taxonomic position of *Renalcis* is controversial, but it is interpreted as red algae, foraminifera and most commonly as

cyanobacteria (Mamet, 1991). Pratt (1984) interpreted *Renalcis* as a 'diagenetic taxa' resulting from the calcification of coccoid blue-green algae grouped in colonies. However, some authors suggested *Renalcis* constitutes fossilized biofilm clusters, resulting

from the calcification process due to the activity of heterotrophic bacteria (Stephens & Sumner, 2002; Turner *et al.* 2000). Woo *et al.* (2008) and Adachi *et al.* (2014) suggested that the *Renalcis* resulted from diagenetic alteration of *Epiphyton* chambers based on their similar structures. However, Luchinina (2009) suggested that the *Renalcis* and *Epiphyton* structures may represent two different steps in the lifecycle of cyanobacteria.

SEM observations of the dark micrite of the *Renalcis* chambers revealed an amorphous flat and translucent mucus-like matrix (Fig. 5a, b, c, d) interpreted by many authors as EPS biofilms (Arp *et al.* 2001; Decho *et al.* 2005; Barrett *et al.* 2009; Mishra *et al.* 2009; Jones, 2011; Zatoń *et al.* 2012; Zhang *et al.* 2015; Mackey *et al.* 2017). Some samples revealed honeycomb-like patterns similar to those observed in modern microbialites (Défarge *et al.* 1994, 1996; Dupraz *et al.* 2009; Spadafora *et al.* 2010). Furthermore abundant bacterial fossils have been described including rod-like bacteria and uniform coccoidal bacteria similar to those reported in modern and ancient microbialites (Perri & Tucker, 2007; Spadafora *et al.* 2010; Perri *et al.* 2012; Shen *et al.* 2017) and usually associated with EPSs. However, in many cases, studied fossils of the probable bacteria in our thrombolite reefs are very small and close to the lowest size boundary for the prokaryotes (Crawford, 2007), but such small, usually coccoid, forms have previously been described from recent and fossil microbialites (Spadafora *et al.* 2010; Perri & Spadafora, 2011).

Our observations suggest a bacterial origin for the *Renalcis* chambers and support the explanation proposed by Stephens & Sumner (2002) and Turner *et al.* (2000) that suggested a bacterial origin for the *Renalcis* group, resulting from the calcification process of EPSs and heterotrophic bacteria. The particular forms of *Renalcis* and *Epiphyton* can be related to the significant difference in bacterial assemblages involved in their formation.

5.b. Origin of micrite

Micrite is widely used to refer to a rock composed of fine-grained calcite crystals (less than 4 µm) produced *in situ* or derived from physical transport and deposition of fine particles (Flügel, 2010). Microscopic study and higher magnification SEM observations of the micromorphological structures allowed us to recognize the autochthonous micrite deposited *in situ* through organomineralization of organic compounds and calcification of bacterial sheaths and EPSs.

5.b.1. Biomineralization

The formation of the Igoudine thrombolites is analogous to that recognized in modern microbialites (Dupraz *et al.* 2004; Perri & Spadafora, 2011) and could involve two major biomineralization processes: (i) replacement of organic matter by biominerals and (ii) calcification or encrustation of bacterial sheaths and EPSs.

Nanoglobules observed in the Igoudine thrombolites are closely associated with EPS relics (Fig. 7a, b, c, e, f), implying their possible origin from anaerobic degradation of EPS biofilms (Aloisi *et al.* 2006; Sánchez-Román *et al.* 2008; Perri *et al.* 2012; Zhang *et al.* 2015). Nanoglobules fuse into variably shaped polyhedrons and micropeloids; similar patterns have been reported in microbial oncoids (Zhang *et al.* 2015). Polyhedrons formed by nanoglobules may have served as primary nuclei for subsequent carbonate crystal growth (Sánchez-Román *et al.* 2008; Spadafora *et al.* 2010; Perri & Spadafora, 2011; Tang *et al.* 2013; Zhang *et al.* 2015). These organominerals can replace the organic part when EPSs and bacterial sheaths have been largely degraded, after the microenvironment

become anoxic or dysoxic (Dupraz *et al.* 2004; Spadafora *et al.* 2010; Perri & Spadafora, 2011; Zhang *et al.* 2015). During this process, precipitation of carbonate minerals happened after intensive decomposition of EPSs and bacterial sheaths so that microbial fossils are rarely preserved (Bartley, 1996; Zhang *et al.* 2015).

Encrustation of bacterial sheaths and EPSs can occur by increasing alkalinity through photosynthetic removal of CO₂ from surrounding waters via photosynthetic prokaryotes and eukaryotic microalgae (Arp *et al.* 2001, 2003; Obst *et al.* 2009). Bacterial sheaths and EPSs previously secreted by bacteria absorb bivalent cations (Ca²⁺, Mg²⁺); the latter decreases the pH of the microenvironment and inhibits carbonate nucleation and precipitation (Dupraz *et al.* 2004; Aloisi *et al.* 2006; Braissant *et al.* 2007). Such a scenario can favour the preservation of EPSs because encrustation happens before advanced microbial organic matter degradation. For carbonate minerals, the primary environmental factor controlling the biomineralization is pH, and an increase in pH induces the carbonate biomineralization (Zhao *et al.* 2020). In the case of possible cyanobacteria, like ancient *Girvanella*, *Epiphyton* and *Renalcis*, photosynthetic uptake of CO₂ and/or HCO₃⁻ could raise pH in ambient waters (Dupraz *et al.* 2004; Zhao *et al.* 2020). On the other hand, heterotrophic bacteria, like sulfate-reducing bacteria at the lower levels of microbial mats, perform ammonification and carbonic anhydrase (CA) catalysis that also raises pH. Moreover, the presence of CA also greatly increases the concentration of bicarbonate in the medium, so that the carbonate minerals reach their saturation state faster (Pan *et al.* 2019; Zhao *et al.* 2020). Increasing alkalinity due to active heterotrophic degradation of organic matter, especially by bacterial sulfate reduction (BSR) communities or other heterotrophic mechanisms, can facilitate mineralization of the bacterial sheaths and EPSs. BSR is active under anoxic to suboxic conditions (Sass *et al.* 2002, 2006); the bicarbonate (HCO₃⁻) produced via BSR can increase the alkalinity of the microenvironment (Dupraz *et al.* 2004; Braissant *et al.* 2007). The presence of pyrite framboids indicates suboxic to anoxic microenvironments where reduction of sulfate occurred in the water column or close to the sediment/seawater interface (Wilkin & Barnes, 1997; Ohfuji & Rickard, 2005; Maclean *et al.* 2008; Zhang *et al.* 2015).

5.b.2. Autochthonous peloidal micrite

Although clotted peloidal micrite is very common within the microbialites, numerous interpretations have been proposed to explain the occurrence of peloid clotted fabrics within the microspar. Cayeux (1935) suggested that clotted fabrics resulted from partial re-crystallization of peloid grains. However, many authors considered that clotted fabrics are bacterial in origin and formed from *in situ* precipitation of calcite during degradation of organic matter mediated by heterotrophic bacteria (Reid, 1987; Sun & Wright, 1989; Riding, 2000). Chafetz (1986) and Riding (2002) noted that the clotted microfabric resembles bacterial colonies that form a microfabric of calcified bacterial biofilms. Similar clotted peloidal micrite has been reported from the Holocene reef microbialites in Tahiti, where lipid biomarkers used in laboratory experiments indicated that a sulfate-reducing bacteria-dominated microbial community degrades the organic matter (Heindel *et al.* 2012). In the thrombolites, a particular 'grainstone-like' peloidal fabric is well developed within the microsparitic matrix (Fig. 4e, f), and higher density and coarse-sized peloids are generally observed close to *Renalcis* chambers. Micro- and nanoscale SEM observations of the matrix show abundant probable irregular calcified bacterial microcolonies that contain clustered rod-like

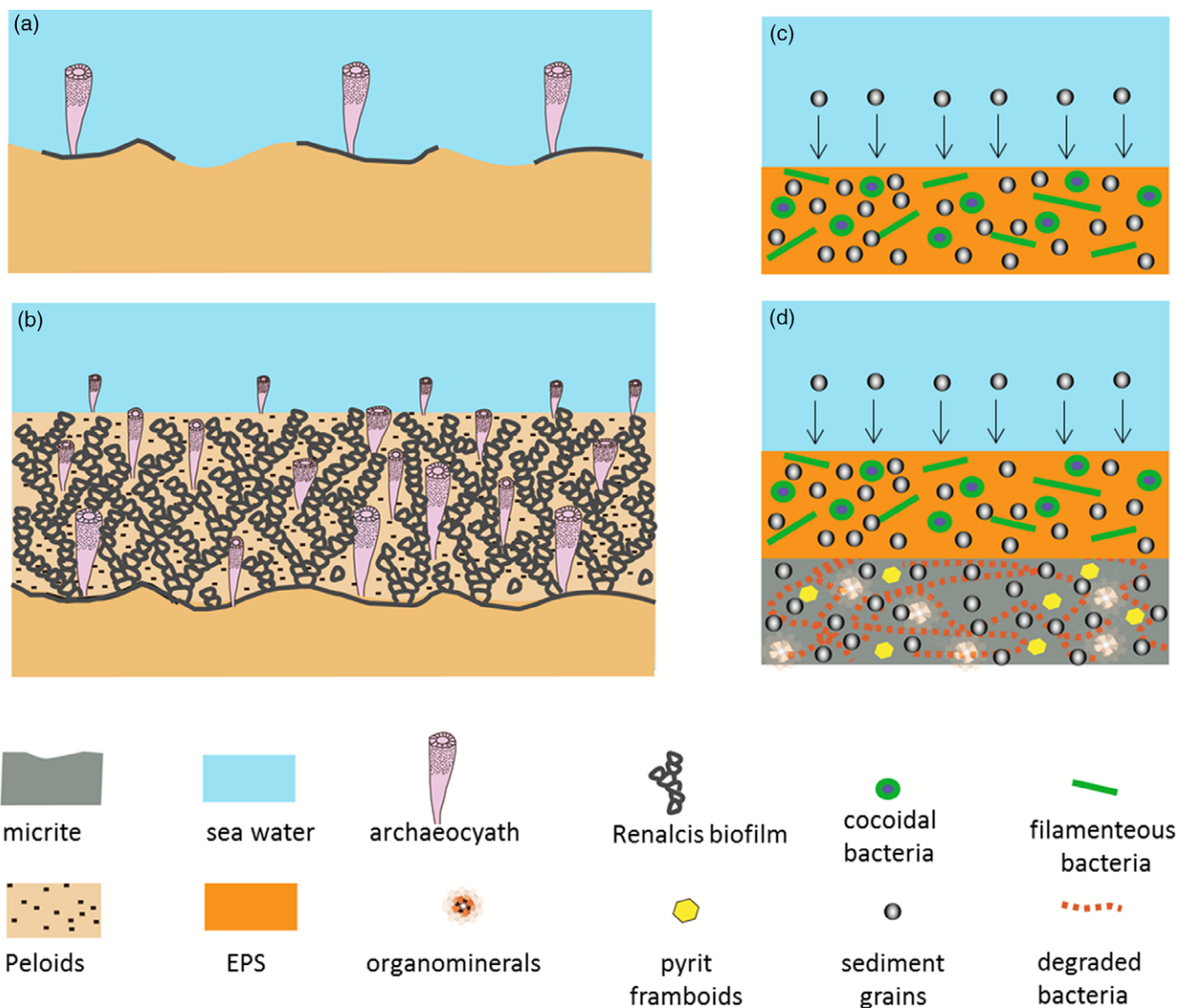


Fig. 10. (Colour online) (a, b) Schematic model showing thrombolite growth and (c, d) EPS mineralization process.

bacteria with associated calcified EPSs and nanoglobules. The size of the colonies is probably controlled by the number of bacteria involved in their formation and the exposure time to seawater before burial by detrital fractions. The higher density of peloids close to *Renalcis* microframes can be explained by a large number of bacteria that are regularly detached from these structures to form new biofilms and colonies. The bacteria associated with *Renalcis* may have consumed its metabolic products.

5.c. Genesis of thrombolites

The Igoudine thrombolitic reefs containing archaeocyaths are interpreted to have developed under favourable conditions for microbial growth such as low siliciclastic input and low hydrodynamic energy with episodic high-energy events. These high-energy events generated numerous surfaces of reef-growth interruption (Fig. 2a, c, d). Under steady conditions, the resulting surfaces were colonized by various microbial populations. EPSs produced by bacteria were accumulated outside the bacterial cells and formed a protective gelatinous film that was used as substrate for

attachment by bacterial colonies (Christensen & Characklis, 1990). EPSs directly promoted the accretion of microbialites by favouring both mineral precipitation (i.e. biologically induced mineralization) and sediment trapping (Riding, 2000). The trapping process can involve simple blockage of grain movement, their adhesion to EPSs and their incorporation (binding) into the mats (Riding, 2000). The latter processes were facilitated where microbial mats had irregular surfaces. On the other hand, smooth films with little surface topography can only incorporate fine-grained particles if they are available (Riding, 2000). *In situ* mineral precipitation (autochthonous micrite) is directly promoted through biogenic mineralization of organic compounds and calcification of bacterial sheaths and EPSs (Fig. 10c, d).

Renalcis with subordinate *Epiphyton* and *Girvanella* dominate the archaeocyaths of the Igoudine Formation thrombolites. *Renalcis* boundstones are the main components of the studied thrombolites (Figs 2c, d, 10a, b). Their cryptic growth habitat is comparable to that of modern cryptic reef biofilms. The growth of *Renalcis* and archaeocyaths was probably synchronous with the influx of fine-grained allochthonous sediments, which are

dominantly micrite and fine-grained microsparite. Archaeocyath skeletons are usually attached to microbial microframes (Fig. 2b, c, d), essentially *Renalcis* dendritic branches, which are in turn encrusted by minor *Epiphyton* chambers and *Girvanella* crusts. Small-sized archaeocyaths filled the remaining space between the *Renalcis* branches (Fig. 2c, d, f), indicating that the available space and the rate of encrustation by the microbial mats likely controlled their growth (Fig. 10a, b). In various examples of early Cambrian thrombolitic reefs containing archaeocyaths, archaeocyaths were considered reef dwellers rather than local framework builders (Debrenne, 2007). However, they could play vital roles in filling the cavities, decreasing water velocity and accelerating the growth of thrombolite reefs, especially under a low rate of sediment supply.

The rate of multiplication and growth of bacteria probably controlled the size of isolated biofilms scattered within the sediments instead of their exposure time before burial by detrital fractions. Bacterial multiplication and the rate of EPS production was likely controlled by the growth of *Renalcis* microframes. Nutrients, oxidant supply and the length of surface exposure can play a primary limiting role for bacterial multiplication (Riding, 2008). The siliciclastic supply increases upwards in the reef complex and reaches up to 35% of the total rock volume (Fig. 9b), essentially above the Amouslek calcareous shales. Thereafter, the growth of thrombolites with archaeocyaths of the Igoudine Formation is stopped by the increase in siliciclastic input. The equilibrium between the EPS production and the sedimentation rate of detrital materials in the environment was likely interrupted when the supply of sediments exceeded a threshold value.

6. Conclusion

The first episode of the Atdabanian reef complex in the western Anti-Atlas consists of tabular and dendritic thrombolites. Small regular and irregular archaeocyaths occur in and around the reefs and are composed of three genera: *Dictyocyathus*, *Erismascosinus* and *Agastrocyathus*. Abundance of archaeocyaths in this horizon does not exceed 20% of the total rock volume. This suggests that archaeocyaths had a subordinate role in reef-building. The thrombolites containing archaeocyaths are dominated by *Renalcis* with subordinate *Epiphyton* and *Girvanella*. Petrographic study and higher resolution SEM observations of the dark micrite of the *Renalcis* chambers showed amorphous translucent sheet-like structures interpreted as EPSs, closely associated with organominerals including nanoglobules and polyhedrons. Exceptionally well-preserved *Renalcis* chambers contain possible bacterial fossils similar to those described in modern microbialites; micro-spherical coccoid fossils and filamentous bacteria coccoid fossils and filamentous tube-like bacteria are observed, isolated or in closely associated colonies, suggesting a bacterial origin for the *Renalcis* calcimicrobe. The growth and expansion of the Igoudine thrombolites took place under favourable conditions such as low hydrodynamic energy and low siliciclastic input.

Acknowledgements. The authors are grateful to Dr Stephen Kershaw and an anonymous reviewer for their constructive and encouraging comments. Financial support for this study was provided by Cadi Ayyad University Morocco; la Région Nouvelle Aquitaine and the University of Poitiers. The authors are grateful to Françoise Debrenne and Adeline Kerner for identifying the archaeocyaths. Lhoussain Ablouh (Centre des analyses chimique, UCA) and Emile Béré from Pole IMAGE UP, University of Poitiers are acknowledged for SEM and EDS analyses. Mouad Akboub, Idir Elhabib and Mouhssin Elhalim are thanked for their assistance during the fieldwork. We also appreciate Claude

and Luis-Marie Bonneval for their warm reception and hospitality in Poitiers. OV was supported by an Estonian Research Council Grant (PRG836), the Sepkoski Grant and a grant by the Institute of Ecology and Earth Sciences, University of Tartu.

Conflict of interest. None.

References

- Adachi N, Nakai T, Ezaki Y and Liu J (2014) Late Early Cambrian archaeocyath reefs in Hubei Province, South China: modes of construction during their period of demise. *Facies* **60**, 703–17.
- Aiken JD (1967) Classification and environmental significance of cryptalgal limestones and dolomites, with illustrations from the Cambrian and Ordovician of southwestern Alberta. *Journal of Sedimentary Research* **37**, 1163–78.
- Aloisi G, Gloter A, Kruger M, Wallmann K, Guyot F and Zuddas P (2006) Nucleation of calcium carbonate on bacterial nanoglobules. *Geology* **34**, 1017–20.
- AlShuaibi AA, Khalaf FI and Al-Zamel A (2015) Calcareous thrombolitic crust on Late Quaternary beachrocks in Kuwait, Arabian Gulf. *Arabian Journal of Geosciences* **8**, 9721–32.
- Álvaro JJ, Benziane F, Thomas R, Walsh GJ and Yazidi A (2014) Neoproterozoic–Cambrian stratigraphic framework of the Anti-Atlas and Ouzellagh promontory (High Atlas), Morocco. *Journal of African Earth Sciences* **98**, 19–33.
- Álvaro JJ and Clausen S (2006) Microbial crusts as indicators of stratigraphic diastems in the Cambrian Micmacca Breccia, Moroccan Atlas. *Sedimentary Geology* **185**, 255–65.
- Álvaro JJ and Debrenne F (2010) The Great Atlasian Reef Complex: an early Cambrian subtropical fringing belt that bordered West Gondwana. *Palaeogeography, Palaeoclimatology, Palaeoecology* **294**, 120–32.
- Álvaro JJ, Ezzouhairi H, Vennin E, Ribeiro ML, Clausen S, Charif A, Ait Ayad N and Moreira ME (2006) The Early-Cambrian Boho volcano of the El Graara massif, Morocco: petrology, geodynamic setting and coeval sedimentation. *Journal of African Earth Sciences* **44**, 396–410.
- Arp G, Reimer A and Reitner J (2001) Photosynthesis-induced biofilm calcification and calcium concentrations in Phanerozoic oceans. *Science* **292**, 1701–4.
- Arp G, Reimer A and Reitner J (2003) Microbialite formation in seawater of increased alkalinity, Satonda Crater Lake, Indonesia. *Journal of Sedimentary Research* **73**, 105–27.
- Barrett J, Spentzos A and Works C (2009) Isolation and characterization of extracellular polymeric substances from micro-algae *Dunaliella salina* under salt stress. *Bioresource Technology* **100**, 3382–6.
- Bartley JK (1996) Actualistic taphonomy of cyanobacteria: implications for the Precambrian fossil record. *Palaio* **11**, 571–86.
- Benssau M and Hamoumi N (2004) Les microbialites de l'Anti-Atlas occidental (Maroc): marqueurs stratigraphiques et témoins des changements environnementaux au Cambrien inférieur. *Comptes Rendus Geosciences* **336**, 109–16.
- Braissant O, Decho AW, Dupraz C, Glunk C, Przekop KM and Visscher PT (2007) Exopolymeric substances of sulfate-reducing bacteria: interactions with calcium at alkaline pH and implication for formation of carbonate minerals. *Geobiology* **5**, 401–11.
- Burne RV and Moore LS (1987) Microbialites: organosedimentary deposits of benthic microbial communities. *Palaio* **2**, 241–54.
- Campbell KA, Francis DA, Collins M, Gregory MR, Campbell SN, Greinert J and Aharon P (2008) Hydrocarbon seep-carbonates of a Miocene forearc (East Coast Basin), North Island, New Zealand. *Sedimentary Geology* **204**, 83–105.
- Cayeux M (1935) *Les Roches Sédimentaire de France: Roche Carbonatées*. Paris: Masson, 463 pp.
- Chafetz HS (1986) Marine peloids; a product of bacterially induced precipitation of calcite *Journal of Sedimentary Petrology* **56**, 812–17.
- Christensen B E and Characklis W G (1990) *Biofilms*. New York: Wiley Interscience.

- Clausen S, Álvaro JJ and Zamora S** (2014) Replacement of benthic communities in two Neoproterozoic–Cambrian subtropical-to-temperate rift basins, High Atlas and Anti-Atlas, Morocco. *Journal of African Earth Sciences* **98**, 72–93.
- Crawford D** (2007) *Deadly Companions: How Microbes Shaped Our History*. Oxford: Oxford University Press.
- Debrenne F** (2007) Lower Cambrian archaeocyathan bioconstructions. *Comptes Rendus Palevol* **6**, 5–19.
- Debrenne F and Debrenne M** (1995) Archaeocyaths of the lower Cambrian of Morocco. *Beringeria Special Issue 2*, 121–45.
- Debrenne F, Gandin A and Courjault-Radé P** (2002) Facies and depositional setting of the Lower Cambrian archeocyath-bearing limestones of southern Montagne Noire (Massif Central, France). *Bulletin de la Société géologique de France* **173**, 533–46.
- Debrenne F, Gandin A and Rowland SM** (1989) Lower Cambrian bioconstructions in northwestern Mexico (Sonora). Depositional setting, paleoecology and systematics of archaeocyaths. *Geobios* **22**, 137–95.
- Decho AW, Visscher PT and Reid RP** (2005) Production and cycling of natural microbial exopolymers (EPS) within a marine stromatolite. *Palaeogeography, Palaeoclimatology, Palaeoecology* **219**, 71–86.
- Défarge C, Trichet J and Coute A** (1994) On the appearance of cyanobacterial calcification in modern stromatolites. *Sedimentary Geology* **94**, 11–19.
- Défarge C, Trichet J, Jaunet AM, Robert M, Tribble J and Sansone FJ** (1996) Texture of microbial sediments revealed by cryo-scanning electron microscopy. *Journal of Sedimentary Research* **66**, 935–47.
- Destombes J, Hollard H and Willefert S** (1985) Lower Palaeozoic rocks of Morocco. In *Lower Palaeozoic Rocks of the World: Lower Palaeozoic of North-Western and West Central Africa: Vol. 4* (ed. CH Holland), pp. 157–84. Chichester: John Wiley and Sons.
- Dupraz C, Reid RP, Braissant O, Decho AW, Norman RS and Visscher PT** (2009) Processes of carbonate precipitation in modern microbial mats. *Earth-Science Reviews* **96**, 141–62.
- Dupraz C, Visscher PT, Baumgartner LK and Reid RP** (2004) Microbe–mineral interactions: early carbonate precipitation in a hypersaline lake (Eleuthera Island, Bahamas). *Sedimentology* **51**, 745–65.
- Flügel E** (2010) *Microfacies of Carbonate Rocks*. Berlin: Springer, 997 pp.
- Gandin A and Debrenne F** (2010) Distribution of the archaeocyath–calcimicrobial bioconstructions on the Early Cambrian shelves. *Palaeoworld* **19**, 222–41.
- Gandin A, Debrenne F and Debrenne M** (2007) Anatomy of the Early Cambrian ‘La Sentinella’ reef complex, Serra Scoris, SW Sardinia, Italy. In *Palaeozoic Reefs and Bioaccumulations: Climatic and Evolutionary Controls* (eds JJ Álvaro, M Aretz, F Boulvain, A Munnecke, D Vachard and E Vennin), pp. 29–50. Geological Society of London, Special Publication no. 275.
- Gandin A and Luchinina V** (1993) Occurrence and environmental meaning of the Early Cambrian calcareous algae of the Tianheban Formation of China (Yangtze Area). In *Studies on Fossil Benthic Algae* (eds F Barattolo, P De Castro and M Parente), pp. 211–17. Società Paleontologica Italiana, Bollettino vol. 1.
- Gasquet D, Ennih N, Liégeois JP, Soulaïmani A and Michard A** (2008) The Pan-African Belt. In *Continental Evolution: The Geology of Morocco* (eds A Michard, O Saddiqi, A Chalouan and D Frizon de Lamotte), pp. 33–64. Berlin: Springer.
- Geyer G and Landing E** (1995) Morocco’95. The Lower–Middle Cambrian standard of Gondwana. *Beringeria Special Issue 2*, 1–171.
- Gischler E, Gibson MA and Oschmann W** (2008) Giant Holocene freshwater microbialites, Laguna Bacalar, Quintana Roo, Mexico. *Sedimentology* **55**, 1293–309.
- Heindel K, Birgel D, Brunner B, Thiel V, Westphal H, Gischler E, Ziegenbalg SB, Cabioch G, Sjöwall P and Peckmann J** (2012) Post-glacial microbialite formation in coral reefs of the Pacific, Atlantic, and Indian Oceans. *Chemical Geology* **304**, 117–30.
- Hofmann HJ** (1973) Stromatolite characteristics and utility. *Earth-Science Review* **9**, 339–73.
- Hupé P** (1960) Sur le Cambrien inférieur du Maroc. In *Report of the 21st International Geological Congress, Norden, Part 8*, pp. 75–85.
- Jahnert RJ and Collins LB** (2012) Characteristics, distribution and morphogenesis of subtidal microbial systems in Shark Bay, Australia. *Marine Geology* **303–306**, 115–36.
- James NP and Gravestock DI** (1990) Lower Cambrian shelf and shelf margin buildups, Flinders Ranges, South Australia. *Sedimentology* **37**, 455–80.
- Jones B** (2011) Biogenicity of terrestrial oncoids formed in soil pockets, Cayman Brac, British West Indies. *Sedimentary Geology* **236**, 95–108.
- Kershaw S, Li Y, Crasquin-Soleau S, Feng Q, Mu X, Collin P-Y, Reynolds A and Guo L** (2007) Earliest Triassic microbialites in the South China block and other areas: controls on their growth and distribution. *Facies* **53**, 409–25.
- Kershaw S, Zhang T and Li Y** (2021) *Calcilobes wangshenghaii* n. gen., n. sp., microbial constructor of Permian–Triassic boundary microbialites of South China, and its place in microbialite classification. *Facies* **67**, 28. doi: [10.1007/s10347-021-00636-x](https://doi.org/10.1007/s10347-021-00636-x).
- Kruse PD, Zhuravlev AY and James NP** (1995) Primordial metazoan–calcimicrobial reefs: Tommotian (Early Cambrian) of the Siberian Platform. *Palaios* **10**, 291–321.
- Laval B, Cady SL, Pollack JC, McKay CP, Bird JS, Grotzinger JP, Ford DC and Bohm HR** (2000) Modern freshwater microbialite analogues for ancient dendritic reef structures. *Nature* **407**, 626–9.
- Luchinina VA** (2009) *Remalcis* and *Epiphyton* as different stages in the life cycle of calcareous algae. *Paleontological Journal* **43**, 463–8.
- Mackey TJ, Sumner DY, Hawes I, Jungblut AD, Lawrence J, Leidman S and Allen B** (2017) Increased mud deposition reduces stromatolite complexity. *Geology* **45**, 663–6.
- Macleán L, Tyliczszak T, Gilbert P, Zhou D, Pray TJ, Onstott TC and Southam G** (2008) A high-resolution chemical and structural study of framboidal pyrite formed within a low-temperature bacterial biofilm. *Geobiology* **6**, 471–80.
- Malooof AC, Schrag DP, Crowley JL and Bowring SA** (2005) An expanded record of Early Cambrian carbon cycling for the Anti-Atlas margin, Morocco. *Canadian Journal of Earth Sciences* **42**, 2195–216.
- Mamet B** (1991) Carboniferous calcareous algae. In *Calcareous Algae and Stromatolites* (ed. R Riding), pp. 370–451. Berlin: Springer.
- Mishra A, Fischer MK and Bäuerle P** (2009) Metal-free organic dyes for dye-sensitized solar cells: from structure: property relationships to design rules. *Angewandte Chemie International Edition* **48**, 2474–99.
- Mobberley JM, Ortega MC and Foster JS** (2012) Comparative microbial diversity analyses of modern marine thrombolitic mats by barcoded pyrosequencing. *Environmental Microbiology* **14**, 82–100.
- Monninger W** (1979) *The Section of Tiout (Precambrian/Cambrian Boundary Beds, Anti-Atlas, Morocco): An Environmental Model*. Würzburg: Arbeiten aus dem Paläontologischen Institut Würzburg vol. 1, 289 pp.
- Myshral KL, Mobberley JM, Green SJ, Visscher PT, Havemann SA, Reid RP and Foster JS** (2010) Biogeochemical cycling and microbial diversity in the thrombolitic microbialites of Highborne Cay, Bahamas. *Geobiology* **8**, 337–54.
- Obst M, Wehrli B and Dittrich M** (2009) CaCO₃ nucleation by cyanobacteria: laboratory evidence for a passive, surface induced mechanism. *Geobiology* **7**, 324–47.
- Ohfuji H and Rickard D** (2005) Experimental syntheses of framboids – a review. *Earth-Science Reviews* **71**, 147–70.
- Pan J, Zhao H, Tucker ME, Zhou J, Jiang M, Wang Y, Zhao Y, Sun B, Han Z and Yan H** (2019) Biomineralization of monohydrocalcite induced by the halophile *Halomonas smyrnensis* WMS-3. *Minerals* **9**, 632. doi: [10.3390/min9100632](https://doi.org/10.3390/min9100632).
- Perri E and Spadafora A** (2011) Evidence of microbial biomineralization in modern and ancient stromatolites. In *Stromatolites: Interaction of Microbes with Sediments* (eds V Tewari and J Seckbach), pp. 631–49. Dordrecht: Springer-Verlag.
- Perri E and Tucker ME** (2007) Bacterial fossils and microbial dolomite in Triassic stromatolites. *Geology* **35**, 207–10.
- Perri E, Tucker ME and Spadafora A** (2012) Carbonate organo-mineral micro- and ultrastructures in sub-fossil stromatolites: Marion Lake, South Australia. *Geobiology* **10**, 105–17.
- Planavsky N and Ginsburg RN** (2009) Taphonomy of modern marine Bahamian microbialites. *Palaios* **24**, 5–24.

- Pratt BR (1984) *Epiphyton* and *Renalcis*; diagenetic microfossils from calcification of coccoid blue-green algae. *Journal of Sedimentary Petrology* **54**, 948–70.
- Puckett MK, McNeal KS, Kirkland BL, Corley ME and Ezell JE (2011) Biogeochemical stratification of carbonate dissolution precipitation in hypersaline microbial mats (Salt Pond, San Salvador, Tha Bahamas). *Aquatic Geochemistry* **17**, 397–418.
- Rees MR, Pratt BR and Rowell AJ (1989) Early Cambrian reefs, reef complexes, and associated lithofacies of the Shackleton Limestone, Transantarctic Mountains. *Sedimentology* **36**, 341–61.
- Reid RP (1987) Nonskeletal peloidal precipitates in Upper Triassic reefs, Yukon Territory (Canada). *Journal of Sedimentary Petrology* **57**, 893–900.
- Riding R (2000) Microbial carbonate: the geological record of calcified bacterial-algal mats and biofilm. *Sedimentology* **47**, 179–214.
- Riding R (2002) Structure and composition of organic reefs and carbonate mud mounds: concepts and categories. *Earth-Science Reviews* **58**, 163–231.
- Riding R (2008) Abiogenic, microbial and hybrid authigenic carbonate crusts: components of Precambrian stromatolites. *Geologia Croatica* **61**, 73–103.
- Riding R (2011) The nature of stromatolites: 3,500 million years of history and a century of research. In *Advances in Stromatolite Geobiology* (eds J Reitner, N-V Quéric and G Arp), pp. 29–74. Berlin: Springer-Verlag.
- Riding R and Zhuravlev AY (1995) Structure and diversity of oldest sponge-microbe reefs: Lower Cambrian, Aldan River, Siberia. *Geology* **23**, 649–52.
- Saadi S, Hilali E, Bensaïd M, Boudda A and Dahmani M (1983) Carte Géologique de Maroc, Scale 1:1,000,000. Rabat: Ministère de l'Énergie et des Mines, Service Géologique du Maroc.
- Sánchez-Román M, Vasconcelos C, Schmid T, Dittrich M, McKenzie JA, Zenobi R and Rivadeneyra MA (2008) Aerobic microbial dolomite at the nanometer scale: implications for the geologic record. *Geology* **36**, 879–82.
- Sass H, Cypionka H and Babenzien H (2006) Vertical distribution of sulfate-reducing bacteria at the oxic-anoxic interface in sediments of oligotrophic Lake Stechlin. *FEMS Microbiology Ecology* **22**, 245–55.
- Sass AM, Eschemann A, Kuhl M, Thar R, Sass H and Cypionka H (2002) Growth and chemosensory behavior of sulfate-reducing bacteria in oxygen–sulfide gradients. *FEMS Microbiology Ecology* **40**, 47–54.
- Schmitt M (1979) *The Section of Tiout (Precambrian/Cambrian Boundary Beds, Anti-Atlas, Morocco): Stromatolites and their Biostratigraphy*. Würzburg: Arbeiten aus dem Paläontologischen Institut Würzburg vol. 2, 188 pp.
- Schmitt M and Monninger W (1977) Stromatolites and thrombolites in Precambrian/Cambrian boundary beds of the Anti-Atlas, Morocco: preliminary results. In *Fossil Algae* (ed. E Flügel), pp. 80–5. Berlin: Springer.
- Shen B, Qin J, Tenger B, Pan A, Yang Y and Bian L (2017) Identification of bacterial fossils in marine source rocks in South China. *Acta Geochimica* **37**, 68–79.
- Spadafora A, Perri E, McKenzie J and Vasconcelos C (2010) Microbial biomineralization processes forming modern Ca:Mg carbonate stromatolites. *Sedimentology* **57**, 27–40.
- Stephens NP and Sumner DY (2002) Renalcids as fossilized biofilm clusters. *Palaïos* **17**, 225–36.
- Sun SQ and Wright VP (1989) Peloidal fabrics in Upper Jurassic reefal limestones, Weald Basin, southern England. *Sedimentary Geology* **65**, 165–81.
- Tang HS, Chen YJ, Santosh M, Zhong H and Yang T (2013) REE geochemistry of carbonates from the Guanmenshan Formation, Liaohe Group, NE Sino-Korean Craton: implications for seawater compositional change during the Great Oxidation Event. *Precambrian Research* **227**, 316–36.
- Tang DJ, Shi XY, Jiang GQ, Pei Y and Zhang W (2012) Mesoproterozoic biogenic thrombolites from the North China platform. *International Journal of Earth Sciences* **102**, 401–13.
- Thomas RJ, Fekkak A, Ennih N, Errami E, Loughlin SC, Gresse PG, Chevallier LP and Liégeois JP (2004) A new lithostratigraphic framework for the Anti-Atlas Orogen, Morocco. *Journal of African Earth Sciences* **39**, 217–26.
- Turner EC, James NP and Narbonne GM (2000) Taphonomic control on microstructure in Early Neoproterozoic reefal stromatolites and thrombolites. *Palaïos* **15**, 87–111.
- Walsh GJ, Benziane F, Aleinikoff JN, Harrison RW, Yazidi A, Burton WC, Quick JE and Saadane A (2012) Neoproterozoic tectonic evolution of the Jebel Saghro and Bou Azzer-El Graara inliers, eastern and central Anti-Atlas Morocco. *Precambrian Research* **216**, 23–62.
- Walter MR and Heys GR (1985) Links between the rise of the metazoan and the decline of stromatolites. *Precambrian Research* **29**, 149–74.
- Wilkin R and Barnes HL (1997) Formation processes of framboidal pyrite. *Geochimica et Cosmochimica Acta* **61**, 323–39.
- Woo J, Chough SK and Han Z (2008) Chambers of *Epiphyton thalli* in microbial buildups, Zhangxia Formation (Middle Cambrian), Shandong Province, China. *Palaïos* **23**, 55–64.
- Zatoń M, Kremer B and Marynowskii L (2012) Middle Jurassic (Bathonian) encrusted oncolites from the Polish Jura, southern Poland. *Facies* **58**, 57–77.
- Zhang WH, Shi X, Jiang G, Tang D and Wang X (2015) Mass-occurrence of oncolites at the Cambrian Series 2–Series 3 transition: implications for microbial resurgence following an early Cambrian extinction. *Gondwana Research* **28**, 432–50.
- Zhao Y, Yan H, Tucker ME, Han M, Zhao H, Mao G, Peng C and Han Z (2020) Calcimicrobes in Cambrian microbialites (Shandong, North China) and comparison with experimentally produced biomineralization precipitates. *Carbonates and Evaporites* **35**, 1–15.